IEEE Access
Multidisciplinary ⋮ Rapid Review ⋮ Open Access Journal

Received July 18, 2021, accepted July 24, 2021, date of publication August 6, 2021, date of current version August 13, 2021.

Digital Object Identifier 10.1109/ACCESS.2021.3103070

FCS-MPC Based Pre-Filtering Stage for Computational Efficiency in a Flying Capacitor Converter

CRISTIAN GARCIA[1], (Member, IEEE), MOHAMMAD MOHAMMADINODOUSHAN[2], (Graduate Student Member, IEEE), VENKATA YARAMASU[2], (Senior Member, IEEE), MARGARITA NORAMBUENA[3], (Senior Member, IEEE), S. ALIREZA DAVARI[4], (Senior Member, IEEE), ZHENBIN ZHANG[5], (Senior Member, IEEE), DAVOOD ARAB KHABURI[6], AND JOSE RODRIGUEZ[7], (Life Fellow, IEEE)

[1]Department of Electrical Engineering, Universidad de Talca, Curico 3340000, Chile
[2]School of Informatics, Computing, and Cyber Systems, Northern Arizona University, Flagstaff, AZ 86011, USA
[3]Department of Electrical Engineering, Universidad Tecnica Federico Santa Maria, Valparaiso 2390123, Chile
[4]Department of Electrical Engineering, Shahid Rajaee Teacher Training University, Tehran 16785-163, Iran
[5]School of Electrical Engineering, Shandong University, Jinan 250061, China
[6]Department of Electrical Engineering, Iran University of Science and Technology, Tehran 1311416846, Iran
[7]Department of Engineering Science, Universidad Andres Bello, Santiago 8370146, Chile

Corresponding author: Cristian Garcia (cristian.garcia@utalca.cl)

This work was supported in part by the Agencia Nacional de Investigación y Desarrollo (ANID) through the Project under Grant Fondecyt 11180235 and Grant ACT192013.

ABSTRACT Finite Control Set Model Predictive Control (FCS-MPC), thanks to its simple and powerful concept, has been applied widely to control the multilevel converters. FCS-MPC allows the control of several objectives and can incorporate restrictions, even nonlinear, into the mathematical model of the system under consideration. However, FCS-MPC needs to evaluate all the switching states of the multilevel converter to find the best switching state to be applied in the next sampling time. For higher-level multilevel converters, this iterative action requires computational capacity that is far beyond the digital controller's capacity in the current market. This paper proposes a new predictive geometric pre-filtering strategy to reduce the iterations and computational burden without affecting the dynamic performance of FCS-MPC. This method consists of a novel pre-filtering stage that uses the predictive model of the system and geometrical properties to find the sector where the reference vector is located and evaluates few vectors that constitute the optimal sector. The proposed method is experimentally validated using a four-level three-cell flying capacitor converter with 512 voltage vectors, obtaining a 64% reduction in the computational burden, while achieving excellent electrical performance indices and maintains the high dynamic performance of the standard FCS-MPC.

INDEX TERMS Computational efficiency, multilevel inverters and predictive control.

I. INTRODUCTION

Finite Control Set Model Predictive Control (FCS-MPC) has been proven, in recent years, as an attractive alternative for controlling power converters in various energy conversion applications [1], [2]. The simplicity and flexibility of the FCS-MPC allows controlling multiple objectives and incorporating restrictions in the cost function.

The associate editor coordinating the review of this manuscript and approving it for publication was Zhilei Yao.

For medium- and high-power applications, the multilevel converters are widely used [3], [4]. The multilevel converters demand handling of different control objectives, which is challenging for classical control strategies with modulation stage [5], [6]. FCS-MPC has been an attractive alternative to control multilevel converters, where the inclusion of two or more control objectives is required; for instance, output current and reactive power regulation [7], DC capacitors voltage balancing [8], selective harmonic elimination [9], switching frequency reduction [10],

common-mode voltage mitigation [11], and semiconductor losses reduction [12].

Despite the simplicity and low implementation cost of FCS-MPC, the multilevel converters impose implementation challenges for FCS-MPC. Given that in FCS-MPC, the system performance should be evaluated by a cost function for all possible switching states to apply the best one to the converter in the next sampling time, the higher number of states lead to high computational burden. The high computational burden is the major hindrance in applying FCS-MPC to multilevel converters. For example, the work in [13] proposes to obtain the vector that minimizes the cost function and evaluate the cost function only for a subset of adjacent vectors. This method reduces the computational burden, however, the dynamic performance of FCS-MPC becomes sluggish because optimal vector could not be found during all the sampling times. In this line, other authors have also chosen to use several criteria to determine the area of adjacency to consider [14], [15], maintaining the problem of finding a sub-optimal solution with low dynamic capacity. The work in [16] reduces computational burden for dead-beat control by evaluating the vectors closest to the reference angularly. This approach has been verified in a direct matrix converter, where the vectors are geometrically distributed in six directions only. It should be noted that geometric division of vectors for multilevel converters is different from matrix converters, because the geometric distribution is homogeneous and in different angular directions for multilevel converters frame. A geometrical division of vectors into sub-regions of the vector space is analyzed in [8] to reduce the computational burden. However, this method requires obtaining a reference through a dead-beat control, evaluating a reduced cost function and not guaranteeing optimal vector calculation during each sampling interval. In the current literature, several other approaches are presented to reduce computational burden of FCS-MPC: 1) use of switching tables based on control objectives to reduce the number of vectors that should be evaluated [17], 2) use of mathematical transformations to obtain an equivalent optimization of the problem even for long prediction horizon [18], 3) consideration of electrical behavior of each switching state and set an error tolerance to consider only some switching states in the evaluation of the cost function [19], 4) use of the dead-beat technique to reduce the number of candidates to be evaluated in the cost function [20]–[22]. All these methods reduce the computational burden, however with some sacrifice in the steady-state and dynamic performance of the converter.

This paper proposes a predictive control strategy with geometric pre-filtering algorithm that divides the space vector of the multilevel converter into six sectors and detects where the reference vector is located. This stage is carried out before the cost function evaluation to reduce the switching states that should be considered in the online optimization. The main advantages of this novel control methods are that it find the optimal vector, same to the standard FCS-MPC, with a significantly computational reduction and thanks to the definition of the sectors has a robustness against calculation errors. Maintaining the characteristic high dynamic performance of FCS-MPC. The proposed method has been validated experimentally using a four-level three-cell Flying Capacitor (FC) converter. The steady-state and transient performance of the proposed method is assessed and compared to the standard FCS-MPC method.

II. MATHEMATICAL MODEL

The four-level FC converter topology is shown in Fig. 1. The FC converter power circuit consists of three series-connected cells. Each cell requires a flying capacitor and two power switches, which operate in a complementary manner for short circuit protection. Fig. 1(a) shows the phase-a power circuit of FC converter, while Fig. 1(b) shows the connections of the three-phase FC converter.

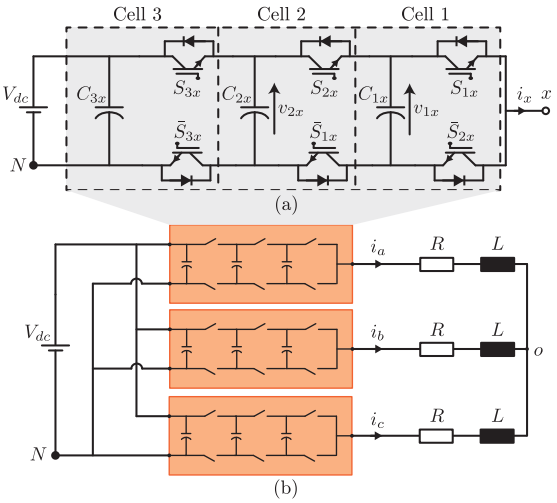

FIGURE 1. Topology of the four-level three-cell flying capacitor converter: (a) 1-phase power circuit and (b) 3-phase connection.

The capacitor voltage ratio is usually set as $v_{x1} : v_{x2} : v_{x3} = 1 : 2 : 3$, with $x \in \{a, b, c\}$. When this condition is met, the converter generates four-level voltage waveform between the output terminal x and the FC converter negative DC terminal N. Under some conditions, this standard ratio can be achieved naturally with a simple Phase-Shifted PWM (PS-PWM) strategy, as detailed in [23], [24]. However, incorporation of other control objectives in PS-PWM is challenging [25], [26].

The output and FC voltages of the three-cell three-phase FC converter (Fig. 1(b)) can be formulated in terms of switching states as,

$$v_{xN} = S_{3x}V_{dc} - (S_{3x} - S_{2x})v_{2x} - (S_{2x} - S_{1x})v_{1x}, \quad (1)$$

$$v_{1x} = v_{1x}(0) + \frac{1}{C_{1x}}\int_0^t i_x(S_{2x} - S_{1x})(\tau)d\tau, \quad (2)$$

$$v_{2x} = v_{2x}(0) + \frac{1}{C_{2x}}\int_0^t i_x(S_{3x} - S_{2x})(\tau)d\tau, . \quad (3)$$

where the possible output voltages and how these are achieved according to the states of the switches are summarized in Table 1.

TABLE 1. Switching states for 1-phase of the FC converter.

State			Output Voltage	Achieved by:
S_{3x}	S_{2x}	S_{1x}	v_{XN}	
0	0	1		v_{1x}
0	1	0	$V_{dc}/3$	$v_{2x} - v_{1x}$
1	0	0		$V_{dc} - v_{2x}$
0	1	1		v_{2x}
1	0	1	$2 \cdot V_{dc}/3$	$V_{dc} - v_{2x} + v_{1x}$
1	1	0		$V_{dc} - v_{1x}$

For an resistive-inductive (RL) load, the output voltage of three-phase FC converter is formulated as,

$$v_{xN} = Ri_x + L\frac{d\,i_x}{dt} + \frac{1}{3}\Big(v_{aN} + v_{bN} + v_{cN}\Big), \tag{4}$$

where R is load resistance, L is load inductance, and i_x is load current. $S_{ix} = 1$ means that the switch is ON and $S_{ix} = 0$ means that switch is OFF for $i \in \{1, 2, 3\}$ and $x \in \{a, b, c\}$. In a rotating $\alpha\beta-$frame with the capacitor voltage ratio set as $1:2:3$, the FC converter has the voltage vector distribution as shown in Fig. 2. This figure also shows the number of redundant vectors.

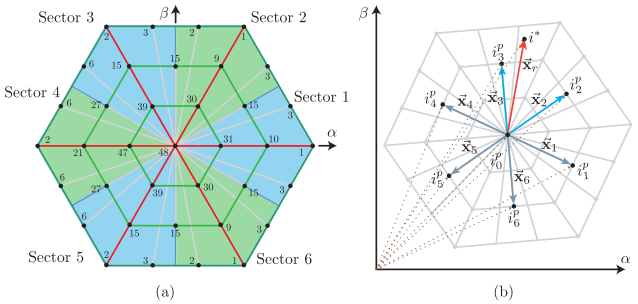

FIGURE 2. Geometrical analysis: (a) Voltage vector in the $\alpha\beta-$frame with the number of the redundant state and defined sectors, and (b) geometrical method in current $\alpha\beta-$frame.

To compensate the computational delay caused by the digital signal processor the cost function is evaluated at the $(k+2)$ instant [27], [28]. The optimal switching state from the previous iteration (k) is used to estimate the variables at $(k+1)$ instant and switching states corresponding to the geometric optimization are used to predict the variables at $(k+2)$ instant. The switching state which minimizes the error at $(k+2)$ instant is selected and applied at sampling instant $(k+1)$. With this approach, one sampling period will be available for calculations. By applying forward Euler approximation, the discrete-time models of FC capacitors voltage for $(k+1)$ instant are obtained from (2) and (3) as follows:

$$v_{1x}^{k+1} = v_{1x}^{k} + \frac{T_s}{C_{1x}}\, i_x^k\big(S_{2x}^{\text{op}} - S_{1x}^{\text{op}}\big), \tag{5}$$

$$v_{2x}^{k+1} = v_{2x}^{k} + \frac{T_s}{C_{2x}}\, i_x^k\big(S_{3x}^{\text{op}} - S_{2x}^{\text{op}}\big), \tag{6}$$

where T_s is control sampling time and superscript op is optimal value in the previous sampling instant.

Similarly, the $(k+2)$ instant FC voltages are obtained as,

$$v_{1x}^{k+2} = v_{1x}^{k+1} + \frac{T_s}{C_{1x}}\, i_x^k\big(S_{2x}^{k} - S_{1x}^{k}\big), \tag{7}$$

$$v_{2x}^{k+2} = v_{2x}^{k+1} + \frac{T_s}{C_{2x}}\, i_x^k\big(S_{3x}^{k} - S_{2x}^{k}\big). \tag{8}$$

The discrete-time model of load currents for $(k+1)$ instant is obtained from (4):

$$i_x^{k+1} = (v_{xN}^{\text{op}} - v_{oN}^{\text{op}})\, K_1 + i_x^k \cdot K_2, \tag{9}$$

where $K_1 = \frac{T_s}{L}$ and $K_2 = \left(1 - \frac{R \cdot T_s}{L}\right)$.

Similarly, the $(k+2)$ instant load current model is obtained as,

$$i_x^{k+2} = (v_{xN}^{k} - v_{oN}^{k})\, K_1 + i_x^{k+1} \cdot K_2. \tag{10}$$

These discrete-time models of three-phase FC converter will be used in the design of predictive current control scheme that will be discussed in the next section.

III. CONTROL STRATEGY

The proposed control scheme is shown in Fig. 3. The proposed control method consists of three major steps, as discussed in subsections III-A, III-B, III-C and III-D.

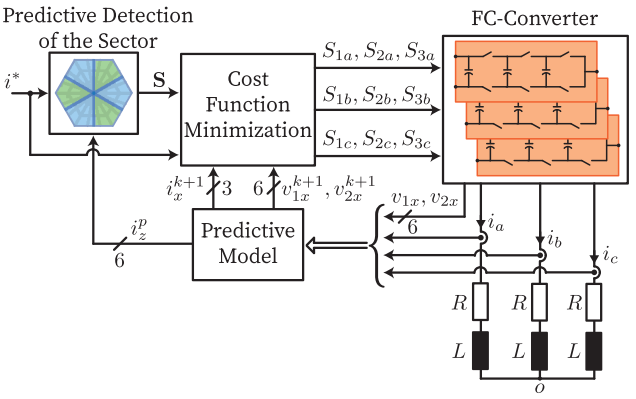

FIGURE 3. Proposed control scheme.

A. GEOMETRICAL SECTORS

The number of voltage vectors of the FC converter to be evaluated by the cost function can be reduced by detecting the location of reference current vector. In this case, it is not necessary to evaluate all the 512 FC vectors; rather, only voltage vectors that are part of the sector where the reference vector is located will be evaluated by the cost function.

This work proposes a strategy for dividing the voltage vector frame (Fig. 2(a)) into six sectors, each for 60 degrees, as shown in Fig. 2. The objective of the geometrical sector detection is to find the location of the reference current vector, but this can be easily used for other control purposes.

Table 2 shows information about the six defined sectors. The information in table contains the initial and final angles of the sectors, related to Fig. 2(a). Furthermore, this table lists the number of active and zero vectors in each sector. The zero

vectors are the same in all sectors. Also, the sum of active and zero vectors evaluated by the cost function is defined as the total vectors column. Finally, the last column lists the percentage reduction of the number of vectors that needs to be evaluated by the cost function with respect to the converter's total number of voltage vectors.

It is important to take into consideration that, the vectors that form the border of adjacent sectors are common for both sectors, just the way zero vectors are considered for all sectors. These two conditions allow the proposed method to be robust to errors of mathematical calculation for cases:

- The reference vector is close to the border of a sector. In this case, due to calculation errors, the proposed method may mislead the detection of the sector between two adjacent sectors. However, the optimal vector is part of the border, and since two adjacent sectors share the set of vectors that make up the border, the proposed method will find the optimal vector.
- If the reference current is close to the predicted current for the zero vector (see Fig. 2(b)), it means that the reference vector $\vec{\mathbf{x}}_r$ (equation 15) has a small magnitude, i.e., it is very close to the origin. In that case, the optimal vector is a zero vector. The method can make an error in detecting the correct sector. However, the optimal vector will be found since all sectors have the set of zero vectors.

Finally, as shown in Table 2, this proposed pre-filtering stage will allow a reduction of less than 36% of the vectors that must be considered in the prediction and evaluation of the cost function. Which produces a reduction of 10734 multiplications and 16984 additions per sampling cycle than standard predictive control that evaluates all states (512), as detailed in Table 3. While the pre-filtering stage only needs 90 multiplications and 72 additions per cycle. It is important to mention that Table 2 is obtained from the spatial division of the vector frame shown in Figure 2, where the zero and active vectors of each sector are quantified according to the definition in degrees given. The last column corresponds to the relationship between all the vectors corresponding to each sector and the total vectors of the converter (512). On the other hand, Table 3 is obtained by quantifying the mathematical operations required by the proposed method and the standard predictive control, where the difference occurs in the pre-filter stage of the proposed method which does not have the standard predictive control and in the number of iterations that the optimal vector search cycle must perform, which for the case of standard predictive control will always be evaluating the 512 states while the one proposed will be a variable according to the total number of states in each sector. Regarding this, it is important to mention 2 things: first that the mathematical operations within the optimization cycle are the same for both methods since that has not been changed; and that Table 3 considered the worst case of the proposed method, that is, sector 4, which has a total of 184, so that any other sector has a lower number of calculations than those presented in Table 3.

TABLE 2. Geometric distribution analysis.

Sector	Angle	Active vectors	Zero vectors	Total vectors	Reduction of calculation
1	330° to 30°	78	48	126	75.39 [%]
2	30° to 90°	75	48	123	75.97 [%]
3	90° to 150°	107	48	155	69.72 [%]
4	150° to 210°	136	48	184	64.06 [%]
5	210° to 270°	107	48	155	69.72 [%]
6	270° to 330°	75	48	123	75.97 [%]

TABLE 3. Comparison of mathematical operations (multiplications (x)-additions (+)).

	Pre-Filtering Stage		Predictions & Cost Function Evaluation		Total	
	15(x)	12(+)	33(x)	52(+)	(x)	(+)
Proposed method	6		184		6162	9640
Standar FCS-MPC	0		512		16896	26624

B. SECTOR DETECTION

The proposed method is based on the division of the $\alpha\beta$ plane into sectors, as shown in Fig. 2(a), which allows to reduce the number of calculations. Therefore, it is essential during each sampling period to find the sector where the reference vector is located. The proposed approach establishes 3 conditions based on vector algebra to effectively detect the sector in which the reference vector is located. In order to detect the location of the reference current vector, the current for seven vectors (six active vectors and one zero vector) are calculated. The active vectors represent the ones located in the border of each sector. The prediction model used in this work is already discussed in section II. To calculate the current vector, the $\alpha\beta$-axis currents are predicted similar to the discrete-time model in (9):

$$i_{z_\alpha} = (V_{aN}(z) - V_{oN}(z))K_1 + i_a K_2, \tag{11}$$

$$i_{z_\beta} = (V_{bN}(z) - V_{oN}(z))K_1 + i_b K_2 + (V_{cN}(z) - V_{oN}(z))K_1 + i_c K_2, \tag{12}$$

where $z \in [0, 6]$ represents the set of six active vectors that are in each of the border of the sectors and the zero vector. They are predicted at the beginning of each sampling period.

The current vector is defined by,

$$i_z^p = i_{z_\alpha} + i_{z_\beta} j. \tag{13}$$

Those that are represented in the Fig. 2(b) with dotted lines. It is important to note that the current predictions are not necessarily centered on the origin of the $\alpha\beta-$frame. The proposed method requires that the zero vector prediction be the center, which is why a new set of vectors is defined as follows,

$$\vec{\mathbf{x}}_z = i_z^p - i_0^p, \tag{14}$$

$$\vec{\mathbf{x}}_r = i^* - i_0^p. \tag{15}$$

This step allows the prediction of the zero vector as the origin, obtaining the vectors $\vec{\mathbf{x}}_z$ that are observed in Fig. 2(b).

Then the proposed method evaluates the following conditions for each of the sectors $S \in [1, 6]$, as follows:

$$C_1(S): \ \vec{\mathbf{x}}_z \cdot \vec{\mathbf{x}}_r > 0, \tag{16}$$

$$C_2(S): \ \vec{\mathbf{x}}_{z+1} \cdot \vec{\mathbf{x}}_r > 0, \tag{17}$$

$$C_3(S): \ (\vec{\mathbf{x}}_z \times \vec{\mathbf{x}}_r) \cdot (\vec{\mathbf{x}}_{z+1} \times \vec{\mathbf{x}}_r) \leq 0. \tag{18}$$

The conditions C_1 and C_2 represent the scalar product of the reference vector with the vectors of each of the edges that make up the sector respectively. If the conditions C_1 and C_2 are true, it means that the reference vector is in the same direction as the vectors that limit the sector. Then, the condition C_3 determines through the calculation of the cross product if the reference vector $\vec{\mathbf{x}}_r$ is between the two vectors that make up the border of the sector.

The last three conditions are integrated into a function that depends on the active vector "z" as follows,

$$f(S) = C_1(S) \ \& \ C_2(S) \ \& \ C_3(S), \tag{19}$$

if $f(S)$ is equal to one, i.e. the conditions $C_1(S)$, $C_2(S)$ and $C_3(S)$ are true, then the current reference is in the sector S, highlighting that the three conditions will be true simultaneously in only one sector.

C. MODEL PREDICTIVE CONTROL

FCS-MPC is used to obtain the voltage vector of the FC converter that tracks reference current and balances the FC capacitors voltage for the three phases of converter. The cost function that fulfills these control objectives is defined as,

$$g_x = \left(i_x^* - i_x^{k+2}\right)^2 + \lambda_{dc}\left(v_{1x}^* - v_{1x}^{k+2}\right)^2 + \lambda_{dc}\left(v_{2x}^* - v_{2x}^{k+2}\right)^2, \tag{20}$$

where λ_{dc} is weighting factor for balancing of FC capacitors voltage. The calculation of weighting factor value is an open research topic [29], [30]. There are different recommendations to determine it, as presented in [31], [32]. In this work the minimum total harmonic distortion (THD) of the current criterion was considered, finding experimentally the value of the weighting factor that produces the lowest THD in the output current while balancing FC voltages within $\pm 2\%$ tolerance range. The cost function in (20) is evaluated for all three phases and incorporated into total cost function as shown below:

$$g = g_A + g_B + g_C. \tag{21}$$

The voltage vector that minimizes the cost function (21) is selected and applied to the FC converter during next sampling time. It must be noted that only the FC vectors that belong to the detected sector are evaluated by the cost function in (21). The vectors that compose each sector are defined in Fig. 2(a), and the quantity of vectors for each sector is defined in Table 2.

The proposed control strategy is shown in Fig. 4. The flowchart is summarized in five simple steps as described below:

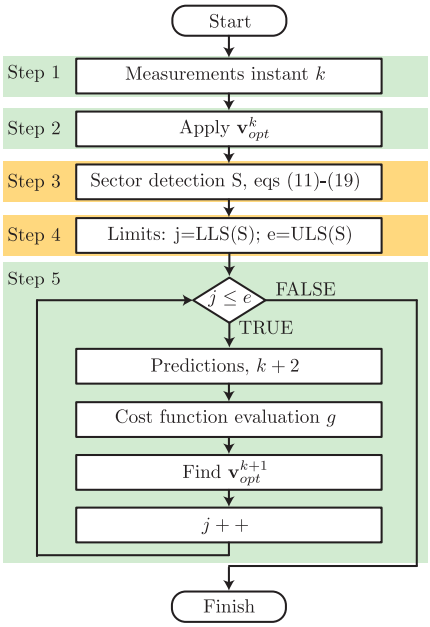

FIGURE 4. Flowchart of the control strategy.

- Step 1, current and voltage measurements are made at the beginning of instant k.
- Step 2, the optimal voltage vector $\mathbf{v}_{opt}^{k}$ determined in the previous period is applied.
- Step 3, the sector S where the reference vector is located is found using the method previously presented.
- Step 4, establishes the limits that the iterative cycle of FCS-MPC will have to cover. These limits group the set of state vectors of each sector $S = \{1, \ldots, 6\}$, they are called Lower Limit of the Sector (LLS(S)) and the Upper Limit of the Sector (ULS(S)).
- Step 5, the iterative cycle of the FCS-MPC is evaluate for find the optimal vector $\mathbf{v}_{opt}^{k+1}$ that will be applied the next sampling time.

Where the steps highlighted in green (steps 1,2 and 5) correspond to the steps of FCS-MPC standard and the steps highlighted in orange (steps 3 and 4) are introduced by this new strategy.

D. IMPLEMENTATION

The implementation of the proposed method considering a real values in one sampling period is shown in this subsection as an practical example. The measurements of the currents and voltages of the capacitors are obtained to predict the currents that describe the limit of the sectors (see Fig. 2(b)) according to equations eq. (11) to (13) as following,

$$i_0^p = -12.27 + j4.92[A] \quad i_4^p = -13.66 + j6.87[A]$$
$$i_1^p = -11.27 + j5.49[A] \quad i_5^p = -13.66 + j5.49[A]$$
$$i_2^p = -11.27 + j6.87[A] \quad i_6^p = -12.45 + j3.54[A]$$
$$i_3^p = -12.45 + j7.56[A]$$

while the reference current in the period is $i^* = -13.95 + j5.02[A]$. With the predictions of i_z^p and the reference i^* is

TABLE 4. Practical evaluation conditions (F=False, T=True).

S	Vector limit		$C_1(S) > 0$		$C_2(S) > 0$		$C_3(S) \leq 0$		$f(S)$
	low	up	value		value		value		
1	$\vec{x}_1$	$\vec{x}_2$	-1.62	F	-1.48	F	3.57	F	F
2	$\vec{x}_2$	$\vec{x}_3$	-1.48	F	0.56	T	14.91	F	F
3	$\vec{x}_3$	$\vec{x}_4$	0.56	T	2.53	T	13.85	F	F
4	$\vec{x}_4$	$\vec{x}_5$	2.53	T	2.39	T	2.56	F	F
5	$\vec{x}_5$	$\vec{x}_6$	2.39	T	0.16	T	-1.91	T	T
6	$\vec{x}_6$	$\vec{x}_1$	0.16	T	-1.62	F	-2.47	T	F

TABLE 5. Parameters of experimental setup.

Parameter	Value	Unit
R	10	[Ω]
L	10	[mH]
$C_{1X} = C_{2X} = C_{3X}$	680	[μF]
v_{dc}	360	[V]
T_s	100	[μs]
λ_{dc}	0.1	

possible to obtain the new vectors,

$$\vec{\mathbf{x}}_1 = 1.0 + j0.57[A] \quad \vec{\mathbf{x}}_4 = -1.39 + j1.95[A]$$
$$\vec{\mathbf{x}}_2 = 1.0 + j1.95[A] \quad \vec{\mathbf{x}}_5 = -1.39 + j0.57[A]$$
$$\vec{\mathbf{x}}_3 = -0.18 + j2.64[A] \quad \vec{\mathbf{x}}_6 = -0.18 - j1.38[A]$$

and the reference vector is,

$$\vec{\mathbf{x}}_r = -1.68 + j0.1[A] \tag{22}$$

Then, the conditions (16) to (19) must to be evaluated. The Table 4 shown the summary of conditions evaluations for the considered sampled period. In this table is possible to observe that the all the conditions are true for the sector 5, this means that only the vectors of the sector 5 (see Fig. 2 and Table 2) will be consider to be evaluated in the cost function (21).

IV. EXPERIMENTAL RESULTS

The proposed method has been validated experimentally and results are presented during steady-state and transient conditions. The FC converter has been built with Semikron SKM75GB12T4 IGBT modules and SKHI22B gate drivers. The parameters used in the experiments are indicated in the Table 5, where DC capacitors are chosen as 2 pu which is best compromise between the size and DC voltage ripples. The control algorithm has been implemented using a host PC running with the MATLAB/Simulink software with real-time interface. The dSPACE DS1103 controller is used to handle the control processes such as sector detection, load current prediction, capacitors voltage estimation, and cost function minimization.

A. PERFORMANCE OF PROPOSED METHOD

Fig. 5 shows the steady-state behavior of the proposed control strategy with a sinusoidal reference current of 12 A(rms) and 50 [Hz] and sampling time $T_s = 100\mu$s. The load currents follow their references with less tracking error, as shown in Fig. 5(a). The phase-*a* FC capacitors voltage are balanced precisely as shown in the top of Fig. 5(b), where the voltages

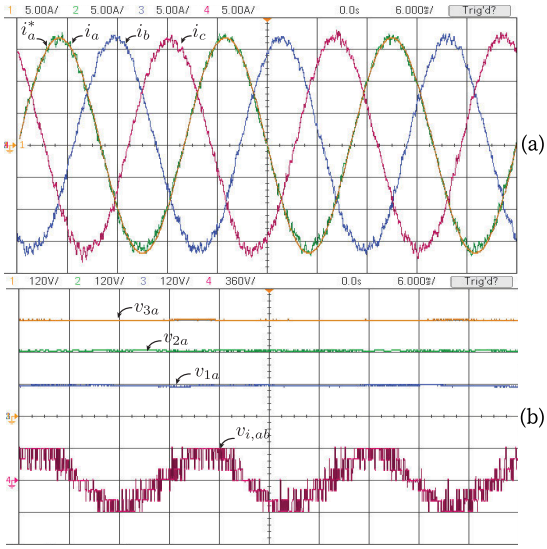

FIGURE 5. Experimental results during steady-state condition: (a) Ch1 - phase-*a* reference current, i_a^* (5A/div), Ch2 - phase-*a* load current, i_a (5A/div), Ch3 - phase-*b* load current, i_b (5A/div), Ch4 - phase-*c* load current, i_c (5A/div). (b) Ch1 - FC3 voltage, v_{3a} (120V/div), Ch2 - FC2 voltage, v_{2a} (120V/div), Ch3 - FC1 voltage, v_{1a} (120V/div), Ch4 - output line-to-line voltage, $v_{i,ab}$ (360V/div).

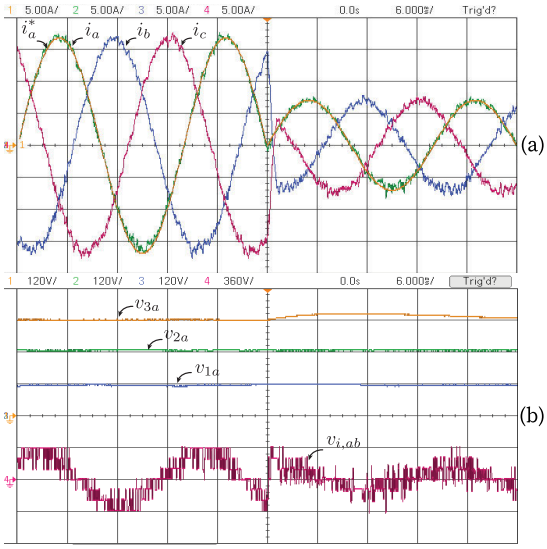

FIGURE 6. Experimental results during a step-change in reference currents: (a) Ch1 - phase-*a* reference current, i_a^* (5A/div), Ch2 - phase-*a* load current, i_a (5A/div), Ch3 - phase-*b* load current, i_b (5A/div), Ch4 - phase-*c* load current, i_c (5A/div). (b) Ch1 - FC3 voltage, v_{3a} (120V/div), Ch2 - FC2 voltage, v_{2a} (120V/div), Ch3 - FC1 voltage, v_{1a} (120V/div), Ch4 - output line-to-line voltage, $v_{i,ab}$ (360V/div).

are constant, keeping 3 : 2 : 1 ratio, without high and low frequency components. Similar behavior is noticed for phase-*b* and *c* capacitors voltage. The converter output line-to-line voltage ($v_{i,ab}$) is presented in the bottom of Fig. 5(b). Due to the balanced capacitors voltage, the FC converter exhibits 7 distinct output voltage levels with less voltage distortion.

Fig. 6 demonstrated the effectiveness of the proposed method in achieving fast dynamic performance during a step-change in reference load currents. The load currents are

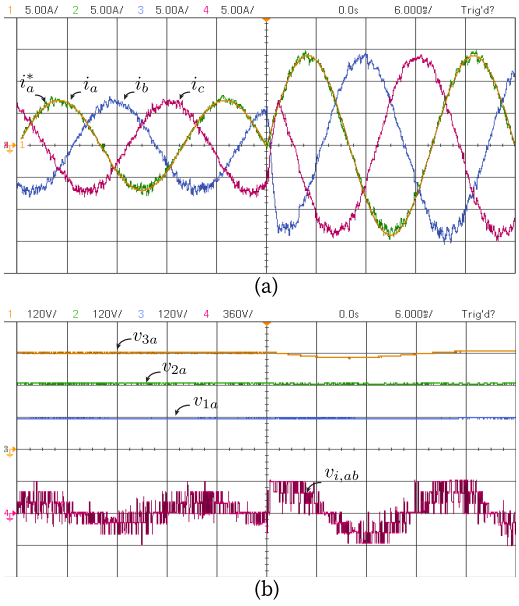

FIGURE 7. Experimental step-up of the proposed control strategy: (a) Ch1 - phase-*a* reference current, i_a^* (5A/div), Ch2 - phase-*a* load current, i_a (5A/div), Ch3 - phase-*b* load current, i_b (5A/div), Ch4 - phase-*c* load current, i_c (5A/div). (b) Ch1 - FC3 voltage, v_{3a} (120V/div), Ch2 - FC2 voltage, v_{2a} (120V/div), Ch3 - FC1 voltage, v_{1a} (120V/div), Ch4 - output line-to-line voltage, $v_{i,ab}$ (360V/div).

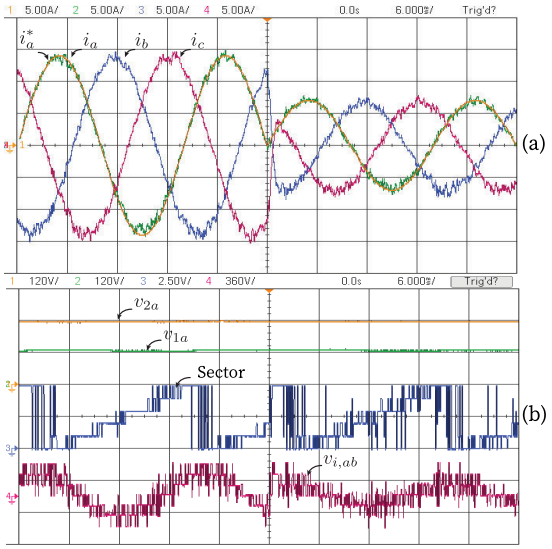

FIGURE 8. Experimental result for the detection of sector: (a) Ch1 - phase-*a* reference current, i_a^* (5A/div), Ch2 - phase-*a* load current, i_a (5A/div), Ch3 - phase-*b* load current, i_b (5A/div), Ch4 - phase-*c* load current, i_c (5A/div). (b) Ch1 - FC2 voltage, v_{2a} (120V/div), Ch2 - FC1 voltage, v_{1a} (120V/div), Ch3 - detected sector (2.5V/div), Ch4 - output line-to-line voltage, $v_{i,ab}$ (360V/div).

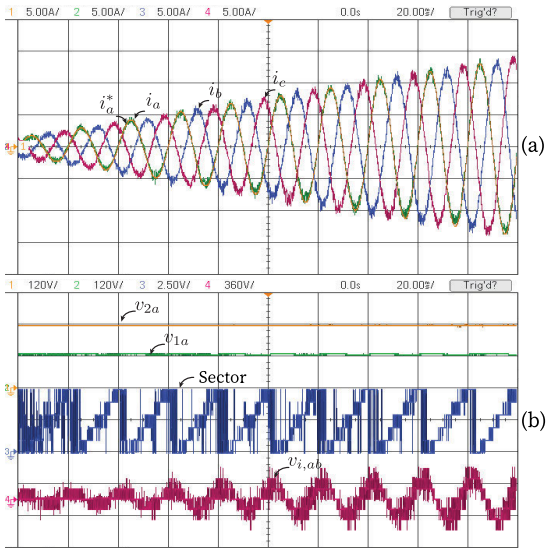

FIGURE 9. Experimental result for the detection of sector: (a) Ch1 - phase-*a* reference current, i_a^* (5A/div), Ch2 - phase-*a* load current, i_a (5A/div), Ch3 - phase-*b* load current, i_b (5A/div), Ch4 - phase-*c* load current, i_c (5A/div). (b) Ch1 - FC2 voltage, v_{2a} (120V/div), Ch2 - FC1 voltage, v_{1a} (120V/div), Ch3 - detected sector (2.5V/div), Ch4 - output line-to-line voltage, $v_{i,ab}$ (360V/div).

shown in Fig. 6(a) with a step change in three-phase reference currents amplitude from 12 A(rms) to -5 A(rms). This figure shows that the output currents track their corresponding references with fast dynamic response and without overshoot. The control of the capacitor voltages is presented in the top of Fig. 6(b), the voltages are stable around their references with a little overshoot in one capacitor (C_{3a}), but it stabilizes in a few milliseconds. The converter output line-to-line voltage is shown in the bottom of Fig. 6(b). During the step change in the reference currents, the voltage levels are decreased from 7 to 5 due to decrease in modulation index. A dynamic response of a step-up current reference is shown in Figure 7. The current reference changes from 5 A(rms) to -12 A(rms). It is observed in Figure 7(a) that the dynamic response is fast and without overshoot dynamic. The voltage of the capacitors, Figure 7(b), remains stable for capacitors 1 and 2, while capacitor 3 has an undershoot voltage for a few milliseconds until it returns to its stable value.

Figs. 8 and 9 show the performance of the proposed method, showing how the sector is calculated at all times during step and ramp change in reference currents, respectively. Fig. 8 shows the performance and sector detection during a step change in reference currents from 10 A(rms) to -5 A(rms). Fig. 9 shows the sector detection during a ramp change in reference currents from 1 A(rms) to 10 A(rms). Fig. 8(b) and 9(b) show the change in sector number from 1 to 6 during step and ramp change in reference currents, verifying the analysis in Fig. 2(a). It is important to mention that in Figs. 8(b) and 9(b) it is possible to see an oscillation between the sectors being selected, this is typical of when the reference is close to the limits of the sectors. Despite this variation, it is positive to note that the redundancy of vectors in the limit of the adjacent sectors helps to prevent the suboptimal vector selection, which is an important advantage of the proposed method.

B. COMPARISON WITH STANDARD FCS-MPC

An experimental comparison between the proposed method and standard FCS-MPC is shown in the Fig. 10. The comparison is performed with $T_s = 320\mu s$, because the standard

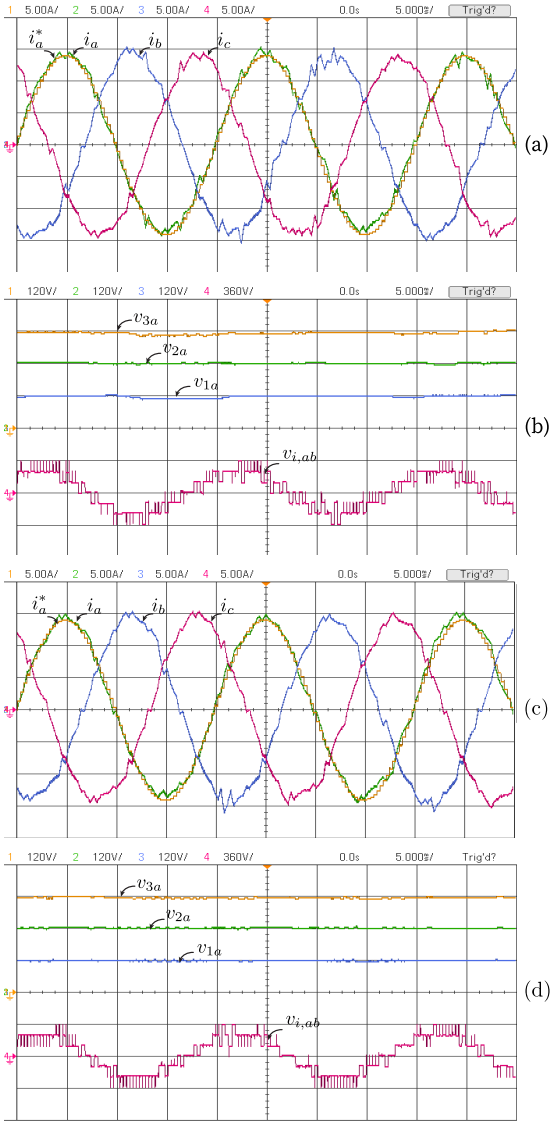

FIGURE 10. Experimental comparison between the proposed control strategy (a)-(b) and standard FCS-MPC (c)-(d): (a)-(c) Ch1 - phase-*a* reference current, i_a^* (5A/div), Ch2 - phase-*a* load current, i_a (5A/div), Ch3 - phase-*b* load current, i_b (5A/div), Ch4 - phase-*c* load current, i_c (5A/div). (b)-(d) Ch1 - FC3 voltage, v_{3a} (120V/div), Ch2 - FC2 voltage, v_{2a} (120V/div), Ch3 - FC1 voltage, v_{1a} (120V/div), Ch4 - output line-to-line voltage, $v_{i,ab}$ (360V/div).

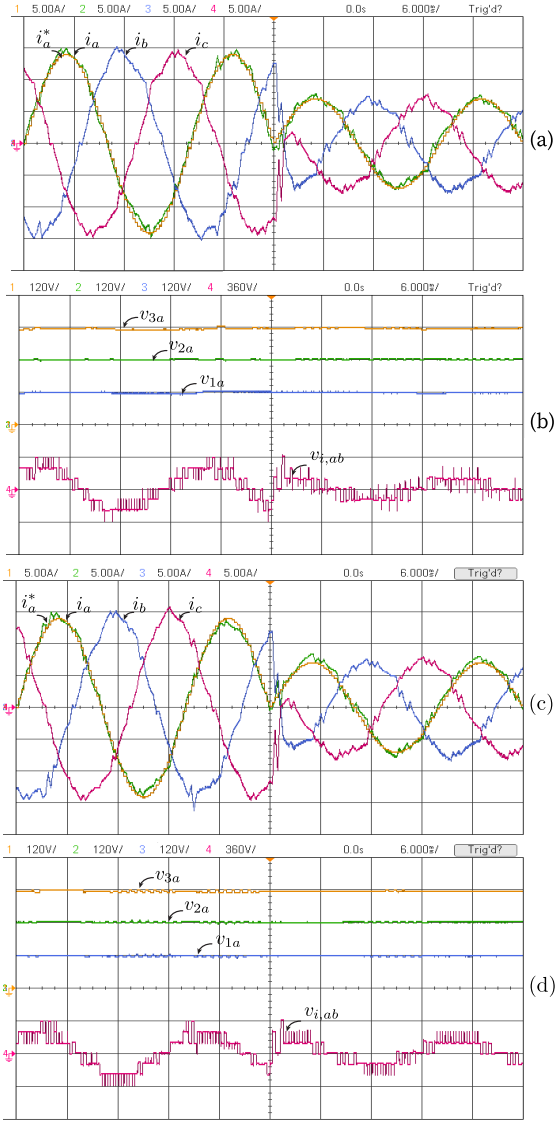

FIGURE 11. Experimental dynamic comparison between the proposed control strategy (a)-(b) and standard FCS-MPC (c)-(d): (a)-(c) Ch1 - phase-*a* reference current, i_a^* (5A/div), Ch2 - phase-*a* load current, i_a (5A/div), Ch3 - phase-*b* load current, i_b (5A/div), Ch4 - phase-*c* load current, i_c (5A/div). (b)-(d) Ch1 - FC3 voltage, v_{3a} (120V/div), Ch2 - FC2 voltage, v_{2a} (120V/div), Ch3 - FC1 voltage, v_{1a} (120V/div), Ch4 - output line-to-line voltage, $v_{i,ab}$ (360V/div).

FCS-MPC requires higher calculation time due to 512 vectors used. The advantage of the proposed method can be clearly understood here because it can implement control algorithm with much smaller sampling times such as $T_s = 100\mu$s. The current waveforms are highly distorted due to very low switching frequency operation. The steady-state behavior of both methods is comparable because the proposed strategy reaches the same solution as FCS-MPC method when evaluating all the possible states of the power converter.

A qualitative analysis of both methods is presented in the Table 6, demonstrating that the performance of both methods is almost identical according to the switching frequency, THD of current, error in reference current tracking, and error in capacitors voltage balancing. These performance indices such as average switching frequency (f_{sw}) of FC converter, THD of load current (THD$_i$), average load current tracking error e_{i_o}, and average capacitors voltage balancing error e_{v_c} are defined in [33].

TABLE 6. Quantitative Performance Comparison.

Performance Indices	Standard FCS-MPC	Proposed FCS-MPC
f_{sw}[Hz]	632	621
THD$_i$[%]	6.68	7.23
e_{i_o}[%]	6.58	6.68
e_{v_c}[%]	0.45	0.60

TABLE 7. Experimental analysis of proposed method.

Performance Indices	Amplitude i^* [A_{RMS}] 1	2	3	4	5	6
f_{sw} [Hz]	2755	2750	2746	2666	2557	2497
THD_i [%]	18.73	9.55	9.45	9.33	9.20	8.39
e_{i_o} [%]	1.75	1.78	2.28	3.24	3.97	4.33
e_{v_c} [%]	0.04	0.06	0.09	0.11	0.14	0.16

Performance Indices	Amplitude i^* [A_{RMS}] 7	8	9	10	11	12
f_{sw} [Hz]	2412	2246	2052	1880	1700	1527
THD_i [%]	7.79	7.05	6.73	6.24	5.66	5.52
e_{i_o} [%]	4.68	4.85	5.20	5.30	5.36	5.52
e_{v_c} [%]	0.18	0.21	0.22	0.24	0.26	0.27

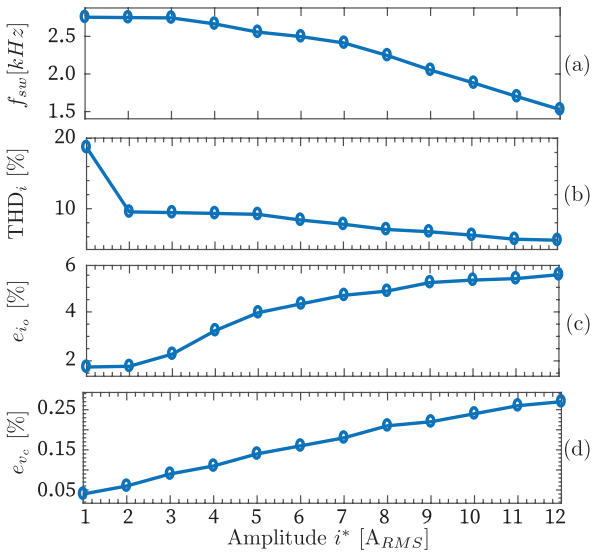

FIGURE 12. Experimental analysis of proposed method: (a) i^* versus f_{sw}; (b) i^* versus THD_i; (c) i^* versus e_{i_o}; (d) i^* versus e_{v_c}.

Comparison between the dynamic performance of the proposed method and the standard FCS-MPC method is shown in the Fig. 11, where the reference load current changes of 10 A(rms) to -5 A(rms) with a frequency of 50[Hz]. Both method achieve the step reference at the same time and with the same waveform behavior.

These results, in steady state and dynamic, show that both methods have an almost equal behavior. The difference in steady state are minimal and are attributed to operating conditions and calculation, since obviously the results are obtained at different times.

C. QUANTITATIVE ANALYSIS OF PROPOSED METHOD

The quantitative analysis of proposed method is presented in Table 7 and Fig. 12 with respect to different values of reference currents i^*. The f_{sw}, THD_i, e_{i_o} and e_{v_c} are presented with respect to different values of i^*. The average switching frequency f_{sw} is noticed to decrease from 2755 Hz to 1527 Hz with the increase in reference currents i^* from 1 A(rms) to 12 A(rms). The THD load current is decreased from 18.73% to 5.52%. The load current tracking error e_{i_o} increased from 1.75% to 5.52%. The capacitors voltage balancing error e_{v_c} is increased slightly from 0.04% to 0.27%.

V. CONCLUSION

This paper presents an experimental validation of a geometrical predictive pre-filtering strategy for a four-level three-cell flying capacitor converter that reduces the computational burden significantly in comparison to the standard FCS-MPC. The proposed control method, using the predictive model of the system, detects at all the times in which sector the reference current vector is located and reduces the iteration number for FCS-MPC scheme. The method obtains a performance very similar to that of standard FCS-MPC, since it finds the same optimal vector that would find standard FCS-MPC when evaluating all possible vectors, maintaining the high dynamic performance that FCS-MPC standard. However, the computational reduction is significant, which allows the proposed method to work with shorter sampling periods and thus obtain a better performance. The proposed strategy reduces the number of vectors that must be evaluated by the cost function between 64.06% and 75.97%, i.e., the strategy only evaluates 36% of the vectors (185 vectors) in the worst case. The experimental results demonstrate excellent performance of the method during steady-state and transient operating conditions.

REFERENCES

[1] S. Vazquez, J. Rodriguez, M. Rivera, L. G. Franquelo, and M. Norambuena, "Model predictive control for power converters and drives: Advances and trends," *IEEE Trans. Ind. Electron.*, vol. 64, no. 2, pp. 935–947, Feb. 2017.

[2] S. Kouro, M. A. Perez, J. Rodriguez, A. M. Llor, and H. A. Young, "Model predictive control: MPC's role in the evolution of power electronics," *IEEE Ind. Electron. Mag.*, vol. 9, no. 4, pp. 8–21, Dec. 2015.

[3] L. Tan, B. Wu, M. Narimani, D. Xu, J. Liu, Z. Cheng, and N. R. Zargari, "A space virtual-vector modulation with voltage balance control for nested neutral-point clamped converter under low output frequency conditions," *IEEE Trans. Power Electron.*, vol. 32, no. 5, pp. 3458–3466, May 2017.

[4] Y. Okazaki, W. Kawamura, M. Hagiwara, H. Akagi, T. Ishida, M. Tsukakoshi, and R. Nakamura, "Experimental comparisons between modular multilevel DSCC inverters and TSBC converters for medium-voltage motor drives," *IEEE Trans. Power Electron.*, vol. 32, no. 3, pp. 1805–1817, Mar. 2017.

[5] A. Edpuganti and A. K. Rathore, "A survey of low switching frequency modulation techniques for medium-voltage multilevel converters," *IEEE Trans. Ind. Appl.*, vol. 51, no. 5, pp. 4212–4228, Sep. 2015.

[6] S. Kouro, M. Malinowski, K. Gopakumar, J. Pou, L. G. Franquelo, B. Wu, J. Rodriguez, M. A. Perez, and J. I. Leon, "Recent advances and industrial applications of multilevel converters," *IEEE Trans. Ind. Electron.*, vol. 57, no. 8, pp. 2553–2580, Aug. 2010.

[7] K. Antoniewicz, M. Jasinski, M. P. Kazmierkowski, and M. Malinowski, "Model predictive control for three-level four-leg flying capacitor converter operating as shunt active power filter," *IEEE Trans. Ind. Electron.*, vol. 63, no. 8, pp. 5255–5262, Aug. 2016.

[8] Z. Zhang, C. M. Hackl, and R. Kennel, "Computationally efficient DMPC for three-level NPC back-to-back converters in wind turbine systems with PMSG," *IEEE Trans. Power Electron.*, vol. 32, no. 10, pp. 8018–8034, Oct. 2017.

[9] R. P. Aguilera, P. Acuna, P. Lezana, G. Konstantinou, B. Wu, S. Bernet, and V. G. Agelidis, "Selective harmonic elimination model predictive control for multilevel power converters," *IEEE Trans. Power Electron.*, vol. 32, no. 3, pp. 2416–2426, Mar. 2017.

[10] J. Ma, W. Song, S. Wang, and X. Feng, "Model predictive direct power control for single phase three-level rectifier at low switching frequency," *IEEE Trans. Power Electron.*, vol. 33, no. 2, pp. 1050–1062, Feb. 2018.

[11] A. Dekka, B. Wu, V. Yaramasu, and N. R. Zargari, "Model predictive control with common-mode voltage injection for modular multilevel converter," *IEEE Trans. Power Electron.*, vol. 32, no. 3, pp. 1767–1778, Mar. 2017.
[12] C. D. Townsend, R. A. Baraciarte, Y. Yu, D. Tormo, H. Z. de La Parra, G. D. Demetriades, and V. G. Agelidis, "Heuristic model predictive modulation for high-power cascaded multilevel converters," *IEEE Trans. Ind. Electron.*, vol. 63, no. 8, pp. 5263–5275, Aug. 2016.
[13] P. Cortes, A. Wilson, S. Kouro, J. Rodriguez, and H. Abu-Rub, "Model predictive control of multilevel cascaded H-bridge inverters," *IEEE Trans. Ind. Electron.*, vol. 57, no. 8, pp. 2691–2699, Aug. 2010.
[14] I. Kim, R. Chan, and S. Kwak, "Model predictive control method for CHB multi-level inverter with reduced calculation complexity and fast dynamics," *IET Electr. Power Appl.*, vol. 11, no. 5, pp. 784–792, May 2017.
[15] Y. Wang, X. Wang, W. Xie, F. Wang, M. Dou, R. M. Kennel, R. D. Lorenz, and D. Gerling, "Deadbeat model-predictive torque control with discrete space-vector modulation for PMSM drives," *IEEE Trans. Ind. Electron.*, vol. 64, no. 5, pp. 3537–3547, May 2017.
[16] M. Siami, D. A. Khaburi, and J. Rodriguez, "Simplified finite control set-model predictive control for matrix converter-fed PMSM drives," *IEEE Trans. Power. Electron.*, vol. 33, no. 3, pp. 2438–2446, Mar. 2018.
[17] M. Habibullah, D. D.-C. Lu, D. Xiao, and M. F. Rahman, "A simplified finite-state predictive direct torque control for induction motor drive," *IEEE Trans. Ind. Electron.*, vol. 63, no. 6, pp. 3964–3975, Jun. 2016.
[18] R. Baidya, R. P. Aguilera, P. Acuña, S. Vazquez, and H. du Toit Mouton, "Multistep model predictive control for cascaded H-bridge inverters: Formulation and analysis," *IEEE Trans. Power Electron.*, vol. 33, no. 1, pp. 876–886, Jan. 2018.
[19] Y. Wang, W. Cong, M. Li, N. Li, M. Cao, and W. Lei, "Model predictive control of modular multilevel converter with reduced computational load," in *Proc. IEEE Appl. Power Electron. Conf. Expo. (APEC)*, Mar. 2014, pp. 1776–1779.
[20] C. Xia, T. Liu, T. Shi, and Z. Song, "A simplified finite-control-set model-predictive control for power converters," *IEEE Trans. Ind. Informat.*, vol. 10, no. 2, pp. 991–1002, May 2014.
[21] C. Sun, D. Sun, Z. Zheng, and H. Nian, "Simplified model predictive control for dual inverter-fed open-winding permanent magnet synchronous motor," *IEEE Trans. Energy Convers.*, vol. 33, no. 4, pp. 1846–1854, Dec. 2018.
[22] H.-C. Moon, J.-S. Lee, and K.-B. Lee, "A robust deadbeat finite set model predictive current control based on discrete space vector modulation for a grid-connected voltage source inverter," *IEEE Trans. Energy Convers.*, vol. 33, no. 4, pp. 1719–1728, Dec. 2018.
[23] R. H. Wilkinson, T. A. Meynard, and H. D. T. Mouton, "Natural balance of multicell converters: The general case," *IEEE Trans. Power Electron.*, vol. 21, no. 6, pp. 1658–1666, Nov. 2006.
[24] A. Ruderman and B. Reznikov, "Five-level single-leg flying capacitor converter voltage balance dynamics analysis," in *Proc. 35th Annu. Conf. IEEE Ind. Electron.*, Nov. 2009, pp. 1–10.
[25] C. Feng, J. Liang, and V. G. Agelidis, "Modified phase-shifted PWM control for flying capacitor multilevel converters," *IEEE Trans. Power Electron.*, vol. 22, no. 1, pp. 178–185, Jan. 2007.
[26] A. M. Y. M. Ghias, J. Pou, G. J. Capella, P. Acuna, and V. G. Agelidis, "On improving phase-shifted PWM for flying capacitor multilevel converters," *IEEE Trans. Power Electron.*, vol. 31, no. 8, pp. 5384–5388, Aug. 2016.
[27] P. Cortes, J. Rodriguez, C. Silva, and A. Flores, "Delay compensation in model predictive current control of a three-phase inverter," *IEEE Trans. Ind. Electron.*, vol. 59, no. 2, pp. 1323–1325, Feb. 2012.
[28] P. Cortés, J. Rodríguez, D. E. Quevedo, and C. Silva, "Predictive current control strategy with imposed load current spectrum," *IEEE Trans. Power Electron.*, vol. 23, no. 2, pp. 612–618, Mar. 2008.
[29] Y. Zhang and H. Yang, "Two-vector-based model predictive torque control without weighting factors for induction motor drives," *IEEE Trans. Power Electron.*, vol. 31, no. 2, pp. 1381–1390, Feb. 2016.
[30] C. A. Rojas, J. Rodriguez, F. Villarroel, J. R. Espinoza, C. A. Silva, and M. Trincado, "Predictive torque and flux control without weighting factors," *IEEE Trans. Ind. Electron.*, vol. 60, no. 2, pp. 681–690, Feb. 2013.
[31] M. Narimani, B. Wu, V. Yaramasu, and N. R. Zargari, "Finite control-set model predictive control (FCS-MPC) of nested neutral point-clamped (NNPC) converter," *IEEE Trans. Power Electron.*, vol. 30, no. 12, pp. 7262–7269, Dec. 2015.
[32] P. Cortes, S. Kouro, B. L. Rocca, R. Vargas, J. Rodriguez, J. I. Leon, S. Vazquez, and L. G. Franquelo, "Guidelines for weighting factors design in model predictive control of power converters and drives," in *Proc. IEEE Int. Conf. Ind. Technol.*, Feb. 2009, pp. 1–7.
[33] V. Yaramasu and B. Wu, *Model Predictive Control of Wind Energy Conversion Systems*. Hoboken, NJ, USA: Wiley, 2017.

CRISTIAN GARCIA (Member, IEEE) received the M.Sc. and Ph.D. degrees in electronics engineering from the Universidad Tecnica Federico Santa Maria, Valparaiso, Chile, in 2013 and 2017, respectively.

He was a Visiting Ph.D. Student with the Power Electronics Machines and Control (PEMC) Group, University of Nottingham, U.K., in 2016. From 2017 to 2019, he was as an Assistant Professor with the Engineering Faculty, Universidad Andres Bello, Santiago, Chile. Since 2019, he has been with the Department of Electrical Engineering, University of Talca, Curico, Chile, where he is currently an Assistant Professor. His research interests include electric transportation applications, variable-speed drives, and model predictive control of power converters and drives.

MOHAMMAD MOHAMMADINODOUSHAN (Graduate Student Member, IEEE) received the M.Sc. degree in electrical engineering. He is currently pursuing the Ph.D. degree in informatics and computing with Northern Arizona University. His past research emphasis was on renewable energy power systems, including data mining, power electronics, and intelligent control. His research interests include electrical engineering for cyber security, including statistics to circuits of memory PUFs, novel password managers utilizing memories, as well as key generation, keyless encryption, and key exchange using memory PUFs.

VENKATA YARAMASU (Senior Member, IEEE) received the B.Tech. degree in electrical and electronics engineering from Jawaharlal Nehru Technological University, Hyderabad, India, in 2005, the M.E. degree in electrical engineering from the S. G. S. Institute of Technology and Science, Indore, India, in 2008, with a focus on power electronics, and the Ph.D. degree in electrical engineering from Ryerson University, Toronto, ON, Canada, in 2014.

From 2014 to 2015, he was a Postdoctoral Research Fellow with the Laboratory for Electric Drive Applications, Research and Center for Urban Energy, Ryerson University. He was with Northern Arizona University, Flagstaff, AZ, USA, in 2015, where he is currently an Assistant Professor of electrical engineering with the School of Informatics, Computing, and Cyber Systems. He has authored or coauthored more than 50 peer-reviewed technical articles, *Model Predictive Control of Wind Energy Conversion Systems* (Wiley-IEEE Press), and more than ten technical reports for the industry. His current research interests include renewable energy, high-power converters, electric vehicles, power quality, and model predictive control.

MARGARITA NORAMBUENA (Senior Member, IEEE) received the B.S. and M.Sc. degrees in electric engineering from the Universidad Tecnica Federico Santa Maria (UTFSM), Valparaiso, Chile, in 2013, the Ph.D. degree *(summa cum laude)* in electronics engineering from the UTFSM, in 2017, and the Doktoringenieur (Dr.-Ing.) degree *(summa cum laude)* from the Technische Universitat Berlin (TUB), in 2018.

She is currently an Assistant Professor with the UTFSM. Her research interests include multilevel converters, model predictive control of power converters and drives, energy storage systems, renewable energy, and electromobility. She received the IEEE IES Student Best Paper Award, in 2019, for her doctoral work. She serves as an Associate Editor for IEEE JOURNAL OF EMERGING AND SELECTED TOPICS IN POWER ELECTRONICS.

S. ALIREZA DAVARI (Senior Member, IEEE) was born in Tehran, Iran, in 1981. He received the M.Sc. and Ph.D. degrees from Iran University of Science and Technology (IUST), Tehran, Iran, in 2006 and 2012, respectively.

From 2010 to 2011, he left for a sabbatical visit at Technische Universitaet Muenchen, Germany. From 2013 to 2020, he was as an Assistant Professor with Shahid Rajaee Teacher Training University, where he has been an Associate Professor. His research interests include encoder-less drives, predictive control, power electronics, and renewable energy.

ZHENBIN ZHANG (Senior Member, IEEE) was born in Shandong, China, in 1984. He received the Ph.D. degree *(summa cum laude)* in electrical engineering from the Institute for Electrical Drive Systems and Power Electronics (EAL), Technical University of Munich (TUM), Munich, Germany, in 2016.

From 2016 to 2017, he was a Research Fellow and the Group-Leader with the Modern Control Strategies for Electrical Drives Group, EAL, TUM. Since 2017, he has been a Full Professor and a Laboratory Director of Shandong University, Jinan, China. Since 2020, he has been the Director of the International Center for Intelligent Energy and Power Conversion Systems, Shandong University. His research interests include power electronics and electrical drives, sustainable energy systems, and smart- and microgrids.

Dr. Zhang received the VDE-Award, Suedbayern, Germany, in 2017. He is an Associate Editor of the IEEE TRANSACTIONS ON INDUSTRIAL ELECTRONICS.

DAVOOD ARAB KHABURI was born in 1965. He received the B.Sc. degree in electronic engineering from Sharif University of Technology, Tehran, Iran, in 1990, and the M.Sc. and Ph.D. degrees in electrical engineering from ENSEM, INPEL, Nancy, France, in 1994 and 1998, respectively. He joined UTC, Compiegne, France, for a period of one year, from 1998 to 1999. Since January 2000, he has been a Faculty Member with the Electrical Engineering Department, Iran University of Science Technology (IUST), where he is currently an Associate Professor. He is one of the founders of Iranian Association of Power Electronics, where he is also a Board Member of this association. He is also a member of Center of Excellence for Power Systems Automation and Operation. He is also the Head of the Power Group, IUST. His research interests include power electronics, motor drives, and digital control.

JOSE RODRIGUEZ (Life Fellow, IEEE) received the Engineer degree in electrical engineering from the Universidad Tecnica Federico Santa Maria, Valparaiso, Chile, in 1977, and the Dr.-Ing. degree in electrical engineering from the University of Erlangen, Erlangen, Germany, in 1985. He has been with the Department of Electronics Engineering, Universidad Tecnica Federico Santa Maria, since 1977, where he was a Full Professor and the President. Since 2015, he has been the President. Since 2019, he has been a Full Professor with the Universidad Andres Bello, Santiago, Chile. He has coauthored two books, several book chapters and more than 400 journal articles and conference papers. His research interests include multilevel inverters, new converter topologies, control of power converters, and adjustable-speed drives. He is a member of the Chilean Academy of Engineering. He received the National Award of Applied Sciences and Technology from the Government of Chile, in 2014. He received the Eugene Mittelmann Award from the Industrial Electronics Society of the IEEE, in 2015. He has received a number of best paper awards from journals of the IEEE. From 2014 to 2020, he has been included in the list of Highly Cited Researchers published by Web of Science.